frontiers in Psychology

ORIGINAL RESEARCH
published: 11 October 2017
doi: 10.3389/fpsyg.2017.01786

Brain Functional Plasticity Driven by Career Experience: A Resting-State fMRI Study of the Seafarer

Nizhuan Wang[1,2], Weiming Zeng[1], Yuhu Shi[1] and Hongjie Yan[3]**

[1] Laboratory of Digital Image and Intelligent Computation, College of Information Engineering, Shanghai Maritime University, Shanghai, China, [2] Neuroimaging Laboratory, School of Biomedical Engineering, Health Science Center, Shenzhen University, Shenzhen, China, [3] Department of Neurology, Affiliated Lianyungang Hospital of Xuzhou Medical University, Lianyungang, China

The functional connectome derived from BOLD resting-state functional magnetic resonance imaging data represents meaningful functional organizations and a shift between distinct cognitive states. However, the body of knowledge on how the long-term career experience affects the brain's functional plasticity is still very limited. In this study, we used a dynamic functional connectome characterization (DBFCC) model with the automatic target generation process K-Means clustering to explore the functional reorganization property of resting brain states, driven by long-term career experience. Taking sailors as an example, DBFCC generated seventeen reproducibly common atomic connectome patterns (ACP) and one reproducibly distinct ACP, i.e., ACP14. The common ACPs indicating the same functional topology of the resting brain state transitions were shared by two control groups, while the distinct ACP, which mainly represented functional plasticity and only existed in the sailors, showed close relationships with the long-term career experience of sailors. More specifically, the distinct ACP14 of the sailors was made up of four specific sub-networks, such as the auditory network, visual network, executive control network, and vestibular function-related network, which were most likely linked to sailing experience, i.e., continuously suffering auditory noise, maintaining balance, locating one's position in three-dimensional space at sea, obeying orders, etc. Our results demonstrated DBFCC's effectiveness in revealing the specifically functional alterations modulated by sailing experience and particularly provided the evidence that functional plasticity was beneficial in reorganizing brain's functional topology, which could be driven by career experience.

Keywords: resting-state fMRI, brain plasticity, career experience, seafarer, dynamic functional connectome

OPEN ACCESS

Edited by:
Sergio Machado, Salgado de Oliveira University, Brazil

Reviewed by:
Mariano Luis Alcañiz Raya, Universitat Politècnica de València, Spain
Lietta Marie Scott, Arizona Department of Education, United States

***Correspondence:**
Weiming Zeng
zengwm86@163.com
Hongjie Yan
yanhjns@gmail.com

Specialty section:
This article was submitted to Quantitative Psychology and Measurement, a section of the journal Frontiers in Psychology

Received: *30 May 2017*
Accepted: *26 September 2017*
Published: *11 October 2017*

Citation:
Wang N, Zeng W, Shi Y and Yan H (2017) Brain Functional Plasticity Driven by Career Experience: A Resting-State fMRI Study of the Seafarer. Front. Psychol. 8:1786. doi: 10.3389/fpsyg.2017.01786

INTRODUCTION

Functional Plasticity and Career Experience

One important issue in cognitive neuroscience concerns the relationship between brain's functional plasticity and individually extensive career training or long-term work experience. In recent years, many studies have demonstrated that blood-oxygen-level-dependent (BOLD) functional magnetic resonance imaging (fMRI) is a powerful modality to help reveal the neural correlates of cognitive

processes in different conditions, such as undergoing a cognitive task, resting-states (Calhoun et al., 2008; Wang et al., 2012, 2013, 2016b; Liu et al., 2013; Ren et al., 2014; Jing et al., 2015; Shi et al., 2015a; Tang et al., 2015; Wang N. et al., 2015) or mental disorders, including psychological subhealth (Shi et al., 2015b), autism spectrum disorder (Ambrosino et al., 2014), dementia (Rytty et al., 2013), and schizophrenia (Du et al., 2015). Recently, it has also been shown that the resting-state functional connectivity in specific regions is modulated by individual behaviors (Hampson et al., 2006), extensive learning (Albert et al., 2009; Tung et al., 2013), and experiences (Jeong et al., 2006; Orr et al., 2014; Wang L. et al., 2015; Shen et al., 2016). Specifically, Shen et al. (2016) noted that there is a significant link between the changes in the time-dependent aspects of resting-state functional connectivity within the vigilance network and long-term driving experiences. Furthermore, Hervais-Adelman et al. (2015) revealed that brain's functional plasticity is associated with the emergence of expertise in extreme language control by exploring the functional response of participants with simultaneous interpretation training. Recently, Yang et al. (2016) demonstrated that the functional connectivity strength among certain paired resting-state networks has the significant changes regarding two resting-state conditions of the professional composers' brain states, i.e., the one before composition task, and the other after composition task. Based on the aforementioned studies, the brain's functional plasticity, as revealed by BOLD fMRI technique, has the potential to elucidate the impact of different types of career training or work experience. However, there is still a lack of knowledge concerning how career training and experience is associated with the dynamics of resting-state functional connectivity, which we seek to address in this study.

Dynamic Functional Connectomes and Brain States

Brain functional connectomes constructed using fMRI data depict the macroscale functional connectivity within the brain (Van Dijk et al., 2010; Sporns, 2011) and have been shown to be powerful in differentiating brain conditions (Lynall et al., 2010). A growing number of reports has also suggested that the brain's functional connectome under resting or task conditions is not static but exhibits complex spatiotemporal dynamics as the brain undergoes dynamic integration, coordination, and responses to internal and external stimuli across multiple time scales (Chang and Glover, 2010; Hutchison et al., 2013; Calhoun et al., 2014). This phenomenon potentially implies that the time-varying dynamic functional connectome (DFC) could offer a more complete description of brain activity in comparison to the static one. For example, Leonardi et al. (2013) used principal component analysis to analyze the DFC in a healthy control group and a disabled relapse-remitting multiple sclerosis (RRMS) group and identified significant connections centered in the default mode network (DMN) with altered contributions in patients. Furthermore, taking advantage of the intrinsic connectivity networks and the corresponding time courses generated by the group ICA (Calhoun et al., 2001), Yu et al. (2015) first constructed DFCs using the intrinsic connectivity networks as nodes and the correlation of sliding time-windowed time courses as edges; then, dynamic graph metrics, such as connectivity strength, clustering coefficients, and global efficiency (Rubinov and Sporns, 2010), were calculated for the healthy group and the schizophrenia group, respectively. Their results demonstrated that the aforementioned measurements in the schizophrenia patients exhibited the lower variances over time in contrast to the healthy group, which provided a new perspective on the pathogenesis of schizophrenia. In addition, based on the brain's dynamic transition and the Fisher discrimination dictionary learning (FDDL) technique (Yang et al., 2014). Zhang et al. (2013) proposed a novel dynamic brain functional connectome characterization model (DBFCC), which successfully extracted the representative atomic connectome patterns (ACP) for the resting and task-related conditions, respectively. Similarly, Li et al. (2014) applied DBFCC to characterize and differentiate the dynamic brain states in the healthy group and the post-traumatic stress disorder group, which also effectively generated two distinct ACPs for the post-traumatic stress disorder group. All of the above studies suggested that DFCs with time-varying information could provide a more accurate description of the brain's activity.

Study Purpose

Inspired by the aforementioned studies, we inferred that the spatiotemporal properties of the DFCs on a finer time scale could potentially provide us with evidence of the relationship between resting-state functional connectivity and career training or long-term experience. The DBFCC model (Zhang et al., 2013; Li et al., 2014) had the advantage of characterizing and differentiating the brain states. However, DBFCC appeared to be vulnerable to the random cluster center selection in K-Means for the clustering of WQCP (whole-brain quasi-stable connectome pattern) samples, which led to randomness and instability in the clustered results. In order to overcome the aforementioned deficiency in DBFCC, the automatic target generation process (ATGP) (Ren and Chang, 2003; Chang et al., 2011) based K-Means clustering for WQCP samples was proposed. Then, to further investigate the relationship between the brain dynamics of resting-state functional connectivity and extensive career training or experience, taking the sailors as an example, we applied the DBFCC with ATGP-K-Means clustering to explore the association between the DFC and sailing experience.

Generally, the seafarers are suitably used to explore the relationship between brain dynamics and career experience due to their occupational stability and professional particularity. For example, a sailor's occupation requires a certain degree of particularity due to the following influencing factors: (1) the marine working environment, a small working space with machinery noise, single-sex colleagues (all male sailors), and long periods of isolation from their families; (2) requirements for good psychological health and strong environmental adaptability; (3) the required maritime professional skills; and (4) strong execution of behavior in a chain of command. Due to the

particularity of a sailor's occupation, we speculate that the long-term sailing experience and career training of seafarers will alter the temporal features of the functional connections among the relevant brain regions, which help to characterize the intrinsic neural substrates of career experience. Also, some common functional connections among specific brain regions regardless of sailing experience, are also maintained as the baseline of dynamic brain function. Thus, we will test this hypothesis as described in the following sections.

The remainder of this paper is organized as follows: the materials' information and framework of DBFCC with ATGP-K-Means clustering are first presented; next, DBFCC is used to explore the common/distinct ACPs between the sailor and non-sailor groups. Finally, the results and analysis are presented together with interpretations, discussion, and conclusions related to the sailors' career training and experience.

MATERIALS AND METHODS

Data Acquisition and Data Preprocessing

Twenty male seafarers [ages: 42–57 years, mean age = 49 years; right handedness] with various positions, such as mate, helmsman, and seaman, were recruited from a shipping company in Shanghai, China. All sailors had approximately 10–20 years of sailing experience. For the non-sailor group, 20 male Chinese participants with matched ages in contrast to the sailors [ages: 48–55 years, mean age = 51 years; right handedness] who worked on land were recruited. All participants were informed about the purpose of this study and signed the written consent form according to procedures approved by the IRB of East China Normal University (ECNU), and none of the participants had a history of neurological and psychiatric disorders. Additionally, all participants did not exhibit abnormalities in the Symptom Checklist-90 (SCL-90) evaluation (Derogatis et al., 1976). The education levels for all the participants were junior college or equivalent, which were matched for two control groups. In data acquisition stage, all participants were instructed to wear ear plugs and to keep their body motionless with their eyes closed, remaining relaxed and awake. The corresponding resting-state BOLD fMRI data for each subject was scanned at the Shanghai Key Laboratory of Magnetic Resonance of ECNU. The concrete acquisition parameters were listed as follows: GE 3.0 Tesla, gradient echo EPI with 36 slices providing whole-brain coverage, number of time points = 160, TR (time of repetition) = 2 s, matrix size = 64 × 64, in-plane resolution = 3.75 mm × 3.75 mm, and slice thickness = 4 mm.

The preprocessing steps for the resting-state fMRI data included slice timing, head motion correction, nuisance covariate (six parameters related to head movement, white matter, and CSF signals) regression, spatial normalization, spatial smoothing with Gaussian kernel of 4 mm, and temporal filtering (0.01–0.08 Hz). After the preprocessing procedure, Craddock's brain atlas with 200 ROIs (region of interest) (Craddock et al., 2012) was used to extract the time series of each ROI for each subject; then, the mean time series of each ROI was used as the reference for each ROI. Craddock's brain atlas is a whole-brain functional atlas established by fMRI data, which seemed to be more suitable to accurately describe brain function than the widely used structural brain atlas, e.g., automated anatomical labeling template (Tzourio-Mazoyer et al., 2002).

Framework of DBFCC

The DBFCC with ATGP-K-Means clustering consisted of five sub-procedures (see P1–P5 depicted in **Figure 1**). The first procedure (P1) was the construction of DFCs, which was based on the Pearson correlation for the sliding time window constrained paired reference time series for any two ROIs in two control groups, i.e., Group 1 and Group 2, depicted in **Figure 1**. Then, the manual segmentation of DFCs (P2) was involved, forming the WQCP sample set (Zhang et al., 2013), which was described in detail in Section "Formation of WQCP Samples." Thirdly, the ATGP-K-Means clustering was proposed to obtain the class labels for each sample in a

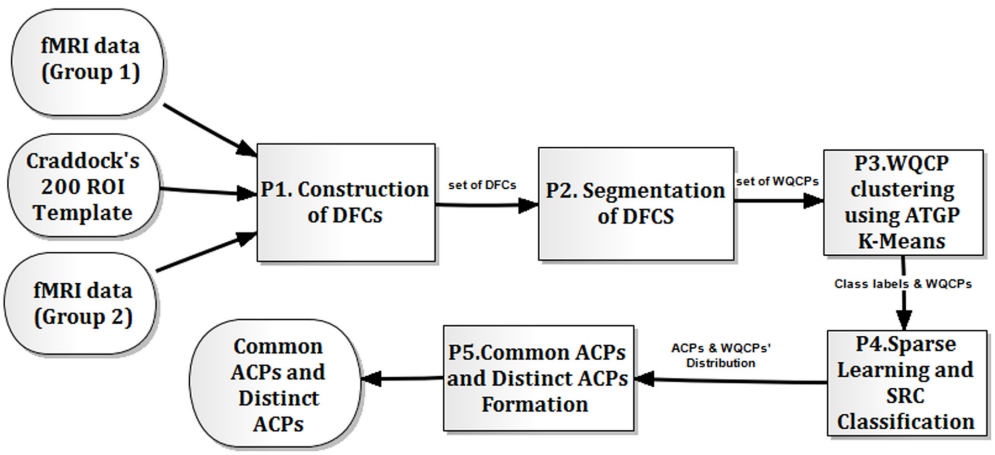

FIGURE 1 | The flow chart of dynamic functional connectome characterization (DBFCC) model with ATGP-K-Means clustering.

WQCP set (P3), which eliminated the resulting randomness of the clustering of K-Means in the original DBFCC (Zhang et al., 2013; Li et al., 2014) (see Section "ATGP-K-Means Clustering on WQCP Set"). Furthermore, the FDDL method (Yang et al., 2014) and the sparse representation based classification (SRC) (Wright et al., 2009) were utilized to generate the ACPs and determine the distributions of the WQCP samples corresponding to each control group under each dictionary class (P4) (see Section "Sparse Learning and SRC Classification"). Finally, the common ACPs and distinct ACPs were classified, based on the ratio distributions of WQCP samples from two groups under the sub-dictionaries generated by FDDL (P5) (see Section "Formation of Common/Distinct ACPs").

Formation of WQCP Samples

The functional connectivity undergoes temporal dynamic transitions (Chang and Glover, 2010; Majeed et al., 2011; Smith et al., 2012; Hutchison et al., 2013; Calhoun et al., 2014), implying that a DFC with more abundant information is better to describe the brain's functional topology than a static one does. Thus, the DFC analysis was adopted in this study. For convenience, we denoted the reference time series for the ith ROI of a specific resting-state fMRI data from Group 1 or Group 2 as $\overline{TS}_i$, $1 \leq i \leq 200$. Specifically, for a given time point t, the functional connectivity between the temporal segments W_i and W_j regarding $\overline{TS}_i$ and $\overline{TS}_j$ was defined as:

$$FC_{i,j,t} = abs\,(correcoef\,(W_i, W_j)),$$
$$FC_{i,j,t} = 0 \text{ if } i = j,\ i, j \in [1, \cdots, 200], \quad (1)$$

where $W_i = [\overline{TS}_{i,t}, \overline{TS}_{i,t+1}, \cdots, \overline{TS}_{i,t+l-1}]$, $W_j = [\overline{TS}_{j,t}, \overline{TS}_{j,t+1}, \cdots, \overline{TS}_{j,t+l-1}]$, and l was the length of the sliding time window (l = 15 with an empirical setting). As the time window slid along the time axis, the DFC was formed as a three-dimensional matrix DFC with dimensions of $200 \times 200 \times (L-l+1)$, in which L denoted the length of $\overline{TS}_i$.

According to prior studies (Zhang et al., 2013; Li et al., 2014), the functional cumulative connectome strength (FCS) was defined as follow:

$$FCS_{i,t} = \sum_{j=1}^{200} DFC_{i,j,t}, \quad (2)$$

where FCS was a matrix with dimensions of $200 \times (L - l + 1)$, and one sample of FCS was depicted in **Figure 2**, in which the horizontal axis represented the time points and the vertical axis denoted the cumulative connectivity strength of each ROI from Craddock's atlas. As shown in **Figure 2**, we found that the FCS consistently maintained a stable connectivity strength in a short period along the horizontal axis. Considering this, we manually divided the whole FCS for each resting-state fMRI data along the time axis into quasi-stable segments (see the dividing black line in **Figure 2**) as suggested in Zhang

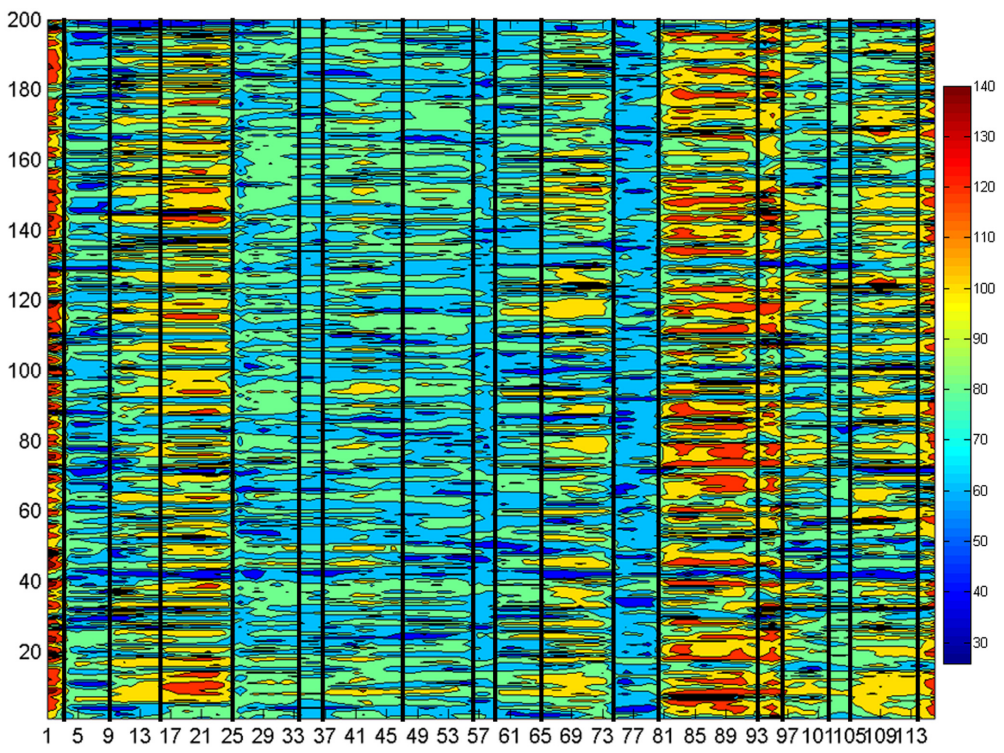

FIGURE 2 | The FCS of the dynamic functional connectome (DFC) for a resting-state functional magnetic resonance imaging (fMRI) sample data.

et al. (2013) and Li et al. (2014), forming the set of WQCP samples.

ATGP-K-Means Clustering on WQCP Set

Each WQCP sample in the WQCP set from Group 1 and Group 2 belonged to different classes, represented by ACPs, which revealed both similar and different functional topologies of the brain dynamics in two control conditions. In DBFCC, the original K-Means clustering was firstly used to categorize the WQCP samples into different classes and each WQCP sample's class label was further retrieved. However, the performance of K-Means was greatly impacted by the randomness of the initial cluster point selection. Thus, in this study, the ATGP algorithm (Ren and Chang, 2003; Chang et al., 2011) was applied to determine the initial cluster points, forming the ATGP-K-Means clustering algorithm. The effectiveness of ATGP in initialization was validated in our previous studies, overcoming the randomness of FastICA (Hyvärinen, 1999; Yao et al., 2013) and improving the accuracy of the separation of brain sources in SDLS (Wang et al., 2016a).

Sparse Learning and SRC Classification

The sparse representation has applied for signal processing, noise suppression (Elad and Aharon, 2006), pattern classification (Huang and Aviyente, 2006), and signal reconstruction (Bruckstein et al., 2009). However, for classification using sparse representation, Huang and Aviyente (2006) noted that reconstructing the signal accurately was not sufficient, while the discrimination of the given signal classes was also important. Based on this idea, the FDDL methodology (Yang et al., 2014) was adopted in this paper to determine the ACPs of resting brain states from the WQCP set. Generally, FDDL fully considered the accuracy of signal reconstruction, the discrimination among the sub-dictionaries and the discrimination of sparse coding coefficients. According to Zhang et al. (2013), FDDL performed better in the determination of ACPs in the WQCP samples than the online sparse dictionary learning algorithm (Mairal et al., 2010). Assuming that all the WQCP samples in two control groups were arranged in a matrix, denoted X, and that ATGP-K-Means clustering had separated the WQCP samples in X into c classes, the FDDL was expressed mathematically as follow:

$$J_{(D,\,S)} = \arg\min_{(D,\,S)}\{r(X, D, S) + \lambda_1\|S\|_1 + \lambda_2 f(s)\}, \tag{3}$$

where the first term $r(X, D, S)$ was the constraint on discriminative fidelity, the second term indicated sparsity constraint, and the last term represented Fisher discriminative constraint of the sparse coding coefficients. Furthermore, $r(X, D, S)$ was expressed as:

$$r(X_i, D, S_i) = \|X_i - DS_i\|_F^2 + \|X_i - D_iS_i^i\|_F^2 + \sum_{\substack{j=1\\ j\neq i}}^{c}\|D_jS_i^j\|_F^2, \tag{4}$$

where $S_i = [S_i^1; \cdots; S_i^j; \cdots; S_i^c]$, S_i^j denoted the coding coefficient of X_i over D_j. In equation (4), the first term was used to enforce the dictionary D with good representative ability for X_i; meanwhile, the other two terms were utilized to showed that the sub-dictionary D_i expressed X_i and the other sub-dictionaries were less to express X_i. Further, the constraint term $f(S)$ was formulated as follows:

$$f(S) = tr(S_W(S)) - tr(S_B(S)) + \eta\|S\|_F^2, \tag{5}$$

$$S_W(S) = \sum_{i=1}^{c}\sum_{s_k\in S_i}(s_k - m_i)\,(s_k - m_i)^T, \tag{6}$$

$$S_B(S) = \sum_{i=1}^{c} n_i(m_i - m)\,(m_i - m)^T, \tag{7}$$

where m_i and m represented the mean vectors of S_i and S, respectively, and n_i indicated the sample number of class X_i. The discriminative coefficient term $f(S)$ here made the dictionary discriminative for the training samples, and was achieved by minimizing the within-class scatter $S_W(S)$ and maximizing the between-class scatter $S_B(S)$ of S. The parameter η was set to 1 for both algorithms' convexity and maximizing the discriminability as described in Yang et al. (2014). The values of the parameters λ_1 and λ_2 were set to 0.01 and 0.02 according to Li et al. (2014), respectively.

In DBFCC, the SRC algorithm (Wright et al., 2009) was used to classify the testing WQCP sample, e.g., x_{test}, which was expressed as

$$\hat{s}_{test} = \arg\min_{s}\left\{\|x_{test} - Ds\|_2^2 + \lambda\|s\|_1\right\}, \tag{8}$$

$$ind = \arg\min_{i}\{e_i\}, \tag{9}$$

where $e_i = \|x_{test} - D_i\hat{s}_i\|_2$, $\hat{s} = [\hat{s}_1; \cdots; \hat{s}_i; \cdots, \hat{s}_c]$ and $\hat{s}_i$ represented the coefficient vectors under the ith sub-dictionary class. Further, in both ATGP-K-Means and FDDL, the Bayesian information criterion (BIC) (Schwarz, 1978) was used to estimate the number of clusters (c), which was also formulated in previous studies (for details, see Zhang et al., 2013; Li et al., 2014).

Formation of Common/Distinct ACPs

Using sparse learning with FDDL for the WQCP sample matrix X, the corresponding dictionary D was extracted, including c sub-dictionaries. Then, the SRC algorithm was used to classify the WQCP samples for each control group, i.e., X_{G1} or X_{G2}, which classified each WQCP sample into a certain sub-dictionary D_i ($1 \le i \le c$). Furthermore, all of the DFCs corresponding to each WQCP for each sub-dictionary (D_i,$1 \le i \le c$) were retrieved, and the corresponding mean functional connectome along the time dimension was calculated, which formed the ACPs with a dimension of 200 × 200 for each sub-dictionary D_i ($1 \le i \le c$). Finally, the c ACPs from Group 1 and Group 2 were generated, respectively.

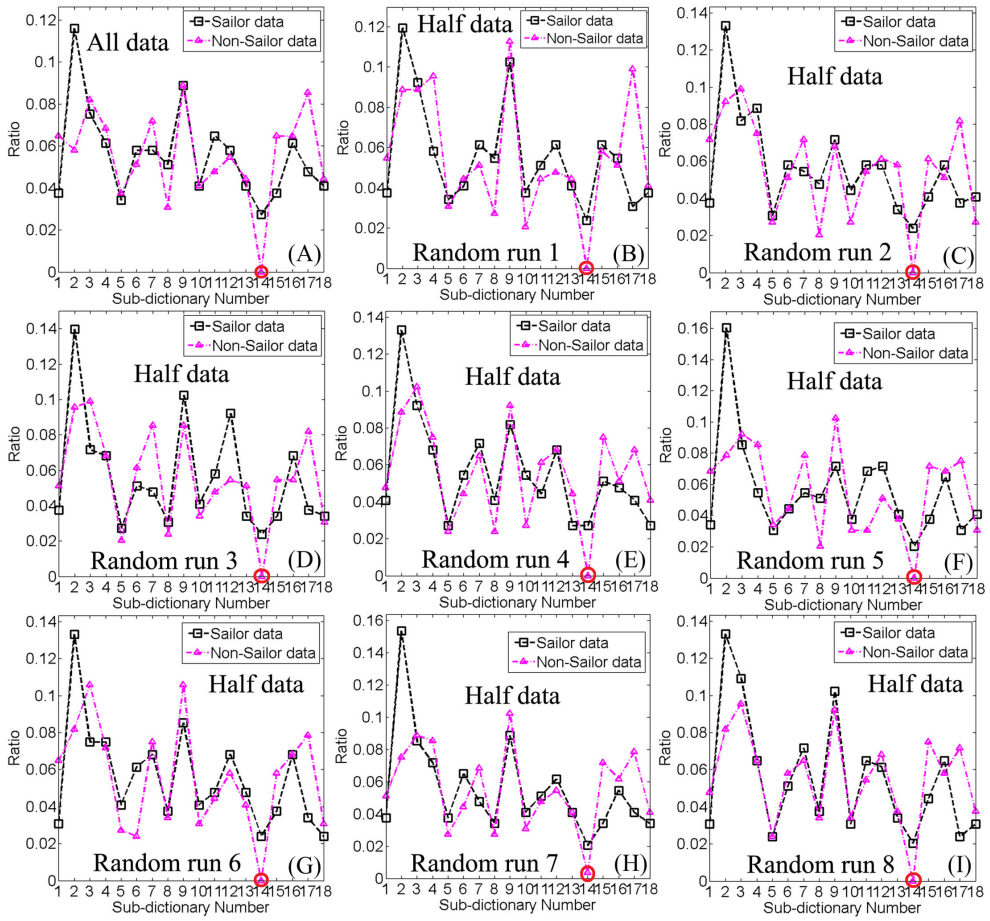

FIGURE 3 | (A) The ratio distributions of WQCPs for the sailor and non-sailor groups under non-resample process; **(B–I)** The ratio distributions of WQCPs for the sailor and non-sailor groups under eight instances of resampling process, respectively. The horizontal axis represents the index of each sub-dictionary, and the vertical axis denotes the ratio distribution of WQCPs under different sub-dictionaries. The circled number on the *x*-axis represents the indexes of distinct atomic connectome patterns (ACPs) between the sailor and non-sailor groups, while the rest denote the indexes of the common ACPs of the two groups.

All the above formed c ACPs could be divided into common ACPs (representing the common brain states) and distinct ACPs (denoting the distinct brain states) regarding two control groups, based on the ratio distributions of WQCP samples from two control groups under the sub-dictionaries generated by FDDL (Li et al., 2014). Namely, some WQCP samples which formed the distinct ACPs, only mostly existed in one certain group. Furthermore, the ACPs should yield high reproducibility and reliability among the resampled WQCP sample sets, i.e., the resampled matrix X_{res}, which could validate effectiveness of the division of common/distinct ACPs. The idea of validation process was simple but heuristic: first, the multiple WQCP subsets (X_{res}) with a half scale in contrast to the WQCP set (X) were generated by the randomly repeated resampling of the WQCP set; then, the FDDL and SRC algorithms were used to perform the sparse learning and classification tasks, respectively, which generated the ratio distributions of the WQCP samples under the variant sub-dictionaries and the corresponding ACPs for each control group; finally, the ratio distributions of the WQCP samples under sampling process for each group could be used to check the previous division of common and distinct ACPs.

RESULTS AND ANALYSIS

The Ratio Distributions of WQCP Set under Resampling Process

Figure 3 depicted the ratio distributions of the WQCP samples corresponding to each control group (sailor group or non-sailor group) under 18 sub-dictionaries generated by FDDL. Specifically, **Figure 3A** showed the ratio distributions of the WQCP samples corresponding to the sailor group or non-sailor group using all WQCP samples for FDDL dictionary learning, while the rest of the sub-figures (**Figures 3B–I**) demonstrated the corresponding sailor group's or non-sailor group's ratio distributions of WQCP samples under eight randomly resampling process. As shown in **Figure 3**, we found that the 18 sub-dictionaries determined by FDDL in both the subsampled WQCP set (X_{res}) and the whole WQCP set (X)

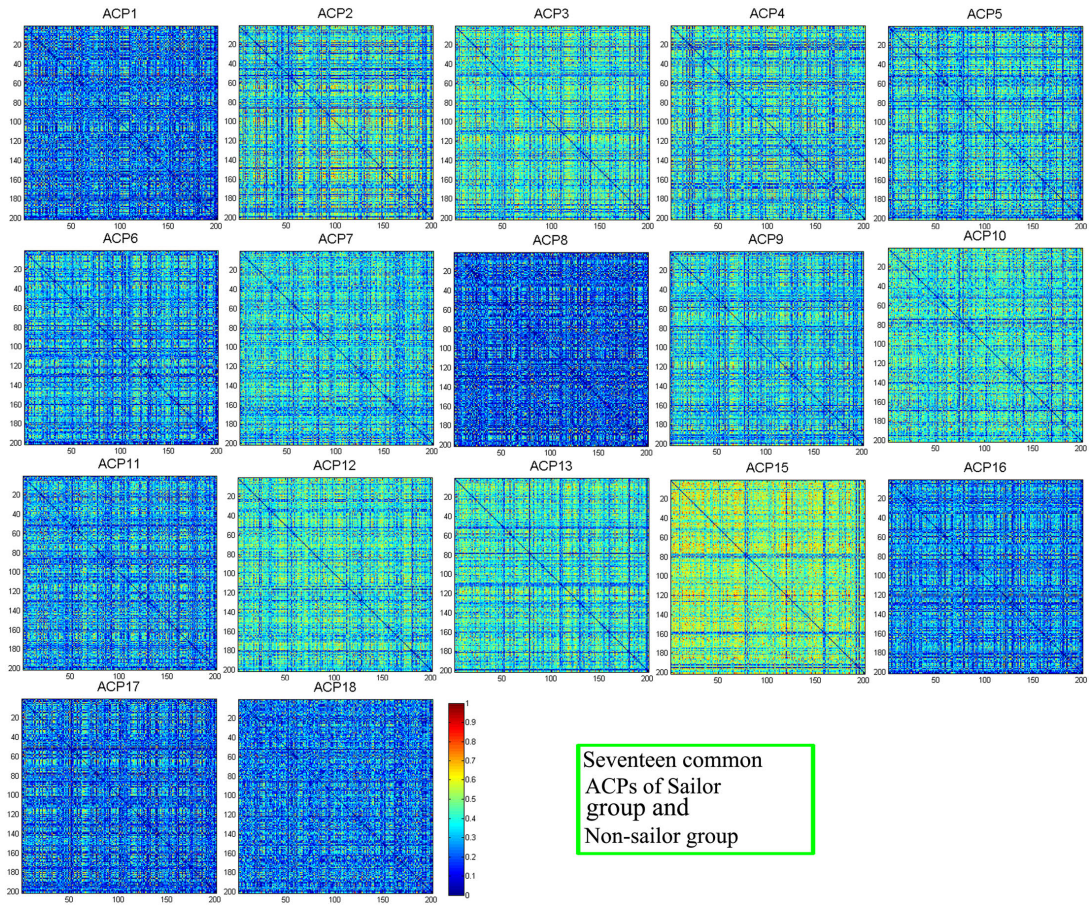

FIGURE 4 | Seventeen common ACPs with a full matrix view for the sailor and non-sailor groups.

exhibited very strong reproducibility and reliability. By observing the ratio distributions of the WQCP samples of each control group in **Figure 3**, we further found that there existed 17 common ACPs and one distinct ACP. Among the 17 common ACPs, the ratio distributions of ACP12 had most consistent difference, implying that compared with the non-sailors, the sailors had a better chance of staying a brain state related to ACP12 as the brain activity went on. This phenomenon demonstrated that the career training with a long period could possibly shape the chances of the brain states where the brain activity belonged to. Besides, the index of the distinct ACP was 14, circled in red along the *x*-axis in each sub-figure of **Figure 3**, as indicated by the significant difference in the ratio distributions for sailor group and non-sailor group. It was noteworthy that the distinct ACP14 exhibited a unique pattern only in the sailor group, and had the potential to play a specific role in this group.

Common/Distinct ACPs

Figure 4 showed the seventeen common ACPs with a full matrix view for both sailor and non-sailor groups. Correspondingly, the 17 common ACPs were projected onto a standard brain surface, as shown in **Figure 5**. Specifically, the connective edges in all common ACPs were retained with a strength larger than 0.75, where the threshold value was also applied in Li et al. (2014).

Figure 6A depicted the distinct ACP14 with a full matrix view, only for the sailor group, while **Figure 6B** showed the connectivity patterns of the distinct ACP14 with strength greater than 0.75, projected onto a standard brain surface. It was noteworthy that ACP14 only existed in the sailor group, which was possibly closely related to the career training and long-term offshore operation of the sailors in contrast to the non-sailors, which was discussed in Section "Distinct ACPs."

DISCUSSION

Common ACPs

In this study, 17 networks were classified as the common ACPs among the sailors and non-sailors (shown in **Figures 4**, **5**), which represented the common functional topology for both control groups. A very important functional network, called DMN, was found in the resting human brain, in which the abnormal or disconnections were often observed with the neuropsychiatric disorders. The DMN was regarded as the potential biomarkers of

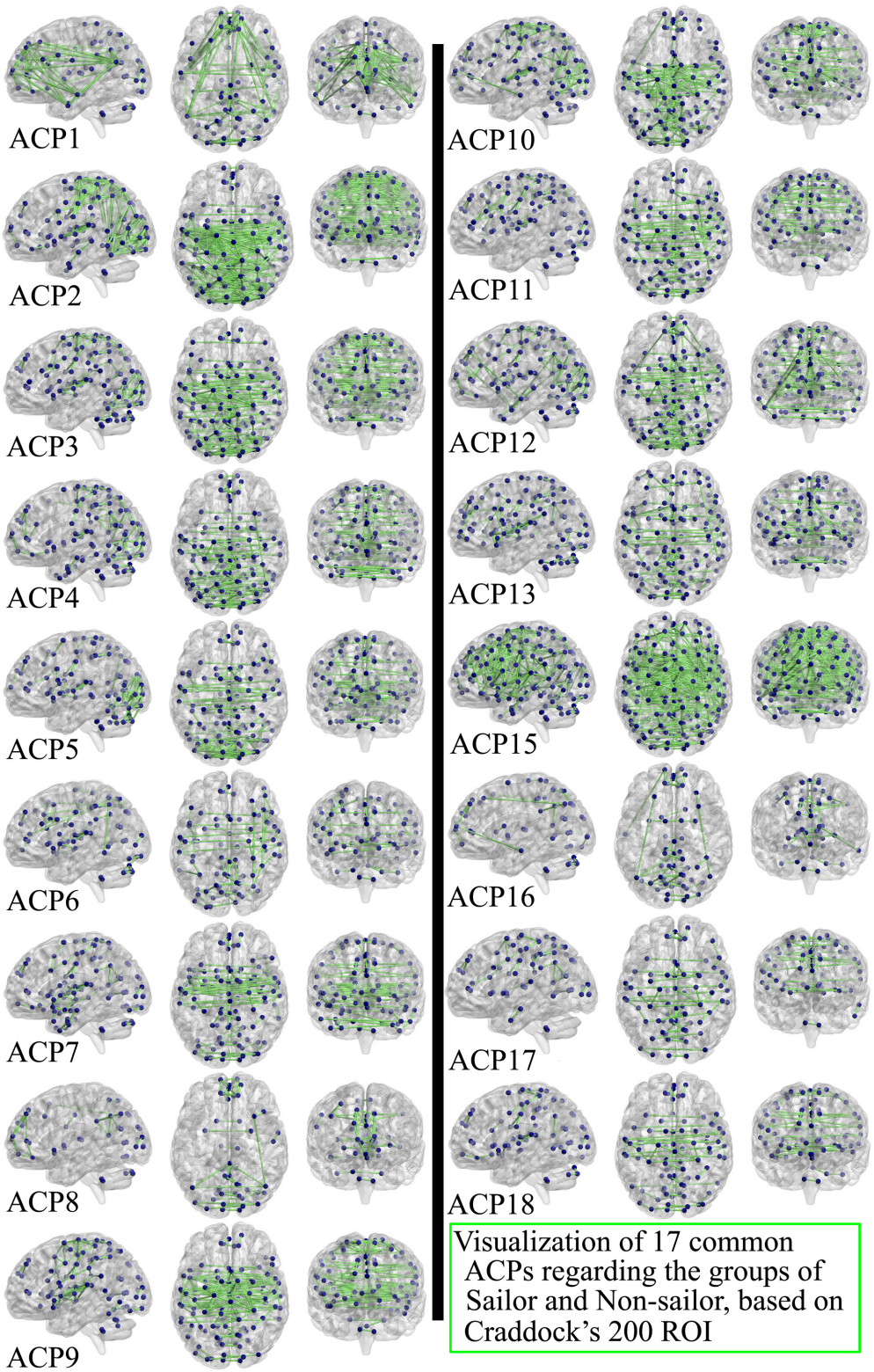

FIGURE 5 | Seventeen common ACPs for the sailor and non-sailor groups, projected onto a standard brain surface. Only the connective edges with strength greater than 0.75 were retained.

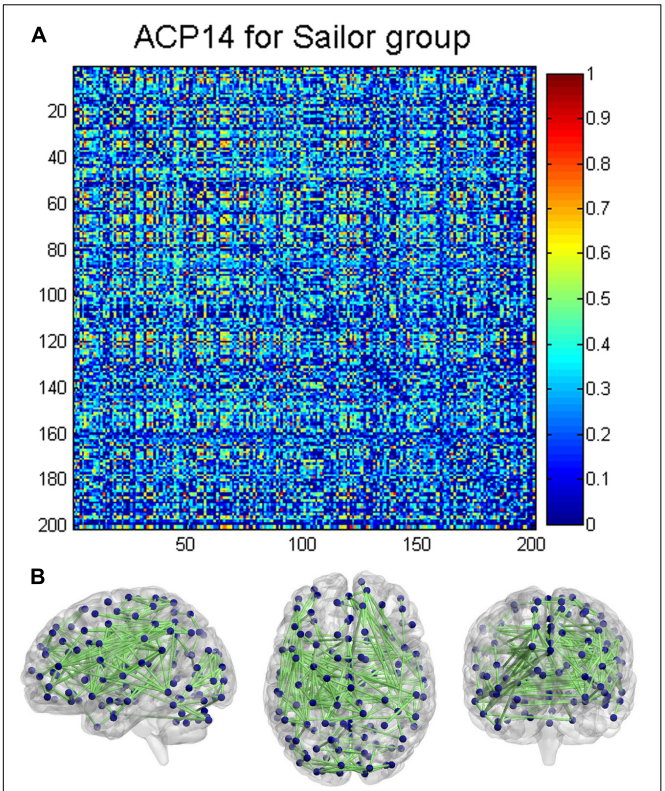

FIGURE 6 | Distinct ACP (ACP14) only existed in the sailor group. **(A)** ACP14 with a full matrix view; **(B)** ACP14 projected onto a standard brain surface. Only the connective edges with strength greater than 0.75 were retained.

neuroimaging in many brain diseases, such as Alzheimer's disease (Greicius et al., 2004), mild cognitive environment (Petrella et al., 2011), depression (Sheline et al., 2009), and schizophrenia (Garrity et al., 2007). According to Raichle et al. (2001), the involved regions include medial prefrontal cortex (MPFC), posterior cingulate cortex (PCC), precuneus, and parietal cortex. The superior frontal cortex, parahippocampal gyrus, inferior temporal cortex, retrosplenial cortex, and cerebellar tonsils could also be considered to be the seed regions for DMN (Fair et al., 2008). On the whole, the common ACPs covered the regions of DMN but there were differences among them, which implied that the DMN functions as a network hub (Liang et al., 2013) in dynamic brain transitions. ACP15 exhibited the highest degree of complexity and the largest number of connections of all brain regions, which justifies why the brain represents 2% of the body's weight but consumes approximately 20% of the calories for the entire body (Raichle and Gusnard, 2002; Zhang and Raichle, 2010). We inferred that ACP15 may represent part of the brain's ongoing activity, which not only supports the maintenance of the neurons' responsiveness for the transient and ever-changing functions of the brain but also initiates sustained functionality (Raichle and Gusnard, 2002). ACP1 was the most similar to DMN with direct connections among the PCC, temporal cortex, precuneus, and MPFC, but was more sparse than ACP12, which was also involved in many connections in the occipital cortex. This provides possible evidence of the exchange of information between DMN and visual network during scanning. Additionally, ACP1 also showed that the DMN exhibited high reproducibility in dynamic brain transitions. In ACP2, ACP3, ACP4, and ACP5, the connections were mostly present in the areas of the parietal lobe and occipital lobe, but ACP4 exhibited connections to the inferior temporal cortex and MPFC. The connections of the two hemispheres were not symmetrical, similar to ACP6, with more connections on the right side. More connections were present on the left side in ACP16 and ACP10. Furthermore, ACP6, ACP8, and ACP16 exhibited more connections within these regions, such as MPFC, precuneus, occipital, and temporal lobes, but were more sparse compared to the rest ACPs. In addition, the connections of ACP7, ACP9, ACP17, and ACP18 mainly covered the sensorimotor, visual, and temporal networks. Finally, regions in the cerebellum were mostly connected with regions in the occipital lobe such as ACP3, ACP5, ACP6, ACP15, and ACP16, while the others exhibited connections inside cerebellum itself.

Distinct ACPs

Using DBFCC model, we identified one distinct ACP, i.e., ACP14 (depicted in **Figure 6**), which obviously denoted different functional topology for both control groups. ACP14 was a characterized ACP of the sailors in contrast to the non-sailors. Many sub-networks were involved in ACP14, such as the auditory network, visual network, executive control network (Beckmann et al., 2005; Damoiseaux et al., 2006; Wang et al., 2012), and vestibular function-related network (Highstein et al., 2004; Angelaki and Cullen, 2008), which implied its complexity and the potential relationship to the seafarers' career experience and professional particularity as discussed below. The auditory network may be associated with the continuous noise disturbances of machines running and ocean sounds. The visual network covered both the basic and advanced visual regions, which possibly implied that the complex sea conditions enforced the combination of the fundamental visual cortex's discovery function and the senior visual cortex's judgment function. The specific functional connections of the basic visual regions and the advanced regions in contrast to the non-sailor group may imply the high efficiency of the dynamic information adjustment of visual circuits. The vestibular function-related network was closely related to the seafarers' occupational training and long-term offshore operations, in which the co-regulatory role of the vestibular system and the visual network allowed the sailors to maintain their body balance and clear vision and improve the ability to determine their own position in three-dimensional space in the maritime environment (Highstein et al., 2004; Angelaki and Cullen, 2008). The executive control network was possibly enhanced by the semi-military training and management (e.g., obeying orders from the captain) of the sailors in the career training stage and the offshore operation stage, which consistently modulated the brain activity of the executive related cortex regions. In summary, the occupational training and long-term offshore experience of the sailors could reorganize the topology of the brain's functional networks in order to accomplish the long-term operation at sea in contrast to the non-sailors on land,

which demonstrated the flexibility in the human brain's functional plasticity.

Limitations and Future Work

There are certain limitations to this study. First, we only considered sailors with long-term sailing experience in excess of 10 years, limiting the number of subjects. Thus, future studies with a larger number of sailors would more definitively explore the functional plasticity driven by career sailing experience. Further, the characterized ACP14 was identified in the sailors with long-term sailing experience. However, whether this factor depended on the duration of sailing experience should be further investigated.

CONCLUSION

The DBFCC model with ATGP-K-Means clustering was effective to characterize the common and different topology of the DFC in sailors and non-sailors. Firstly, the reproducible common ACPs shared by the sailors and non-sailors implied that common dynamic transition states existed, possibly as the functional transition baseline of the human brain. Furthermore, we found that the brain's functional plasticity could be modulated by the longer-term career sailing experience. Stated concretely, one reproducible distinct ACP of the sailors in contrast to the non-sailors showed a close relationship to long-term sailing training and experience, which was the potential to be as a biomarker to characterize the sailors' functional brain. Our findings provide the evidence of that how the sailing experience could influence the dynamic functional reorganization in the healthy human brain to satisfy the professional particularity. Also, this study demonstrates the effectiveness of the revised DBFCC model, which potentially has wide applicability in the exploration of the functional plasticity driven by other types of career training and experience.

AUTHOR CONTRIBUTIONS

Collection of fMRI data: NW, WZ, and YS. Design of the work: NW, HY, and WZ. Analysis and interpretation: NW, HY, WZ, and YS. Drafting the article: NW, HY, and WZ.

ACKNOWLEDGMENTS

This work was supported by the National Natural Science Foundation of China (Nos. 61701318, 31170952, and 31470954), the Shanghai Science and Technology Committee Program (No. 14590501700), the Programs for Graduate Special Endowment Fund for Innovative developing (No. 2013ycx072), and Excellent Doctoral Dissertation Cultivation (No. 2013bxlp003) of Shanghai Maritime University, the Natural Science Foundation of SZU (No. 2017088) and the Guangdong Provincial Medical Science and Technology Research Fund (No. A2017038).

REFERENCES

Albert, N. B., Robertson, E. M., and Miall, R. C. (2009). The resting human brain and motor learning. *Curr. Biol.* 19, 1023–1027. doi: 10.1016/j.cub.2009.04.028

Ambrosino, S., Bos, D. J., van Raalten, T. R., Kobussen, N. A., van Belle, J., Oranje, B., et al. (2014). Functional connectivity during cognitive control in children with autism spectrum disorder: an independent component analysis. *J. Neural Transm.* 121, 1145–1155. doi: 10.1007/s00702-014-1237-8

Angelaki, D. E., and Cullen, K. E. (2008). Vestibular system: the many facets of a multimodal sense. *Annu. Rev. Neurosci.* 31, 125–150. doi: 10.1146/annurev.neuro.31.060407.125555

Beckmann, C. F., DeLuca, M., Devlin, J. T., and Smith, S. M. (2005). Investigations into resting-state connectivity using independent component analysis. *Philos. Trans. R. Soc. Lond. B Biol. Sci.* 360, 1001–1013. doi: 10.1098/rstb.2005.1634

Bruckstein, A. M., Donoho, D. L., and Elad, M. (2009). From sparse solutions of systems of equations to sparse modeling of signals and images. *SIAM Rev.* 51, 34–81. doi: 10.1137/060657704

Calhoun, V. D., Adali, T., Pearlson, G. D., and Pekar, J. J. (2001). A method for making group inferences from functional MRI data using independent component analysis. *Hum. Brain Mapp.* 14, 140–151. doi: 10.1002/hbm.1048

Calhoun, V. D., Kiehl, K. A., and Pearlson, G. D. (2008). Modulation of temporally coherent brain networks estimated using ICA at rest and during cognitive tasks. *Hum. Brain Mapp.* 29, 828–838. doi: 10.1002/hbm.20581

Calhoun, V. D., Miller, R., Pearlson, G., and Adali, T. (2014). The chronnectome: time-varying connectivity networks as the next frontier in fMRI data discovery. *Neuron* 84, 262–274. doi: 10.1016/j.neuron.2014.10.015

Chang, C., and Glover, G. H. (2010). Time–frequency dynamics of resting-state brain connectivity measured with fMRI. *Neuroimage* 50, 81–98. doi: 10.1016/j.neuroimage.2009.12.011

Chang, C. I., Xiong, W., Chen, H. M., and Chai, J. W. (2011). Maximum orthogonal subspace projection approach to estimating the number of spectral signal sources in hyperspectral imagery. *IEEE J. Sel. Top. Signal Process.* 5, 504–520. doi: 10.1109/JSTSP.2011.2134068

Craddock, R. C., James, G. A., Holtzheimer, P. E., Hu, X. P., and Mayberg, H. S. (2012). A whole brain fMRI atlas generated via spatially constrained spectral clustering. *Hum. Brain Mapp.* 33, 1914–1928. doi: 10.1002/hbm.21333

Damoiseaux, J. S., Rombouts, S. A. R. B., Barkhof, F., Scheltens, P., Stam, C. J., Smith, S. M., et al. (2006). Consistent resting-state networks across healthy subjects. *Proc. Natl. Acad. Sci. U.S.A.* 103, 13848–13853. doi: 10.1073/pnas.0601417103

Derogatis, L. R., Rickels, K., and Rock, A. F. (1976). The SCL-90 and the MMPI: a step in the validation of a new self-report scale. *Br. J. Psychiatry* 128, 280–289. doi: 10.1192/bjp.128.3.280

Du, Y., Pearlson, G. D., Liu, J., Sui, J., Yu, Q., He, H., et al. (2015). A group ICA based framework for evaluating resting fMRI markers when disease categories are unclear: application to schizophrenia, bipolar, and schizoaffective disorders. *Neuroimage* 122, 272–280. doi: 10.1016/j.neuroimage.2015.07.054

Elad, M., and Aharon, M. (2006). Image denoising via sparse and redundant representations over learned dictionaries. *IEEE Trans. Image Process.* 15, 3736–3745. doi: 10.1109/TIP.2006.881969

Fair, D. A., Cohen, A. L., Dosenbach, N. U., Church, J. A., Miezin, F. M., Barch, D. M., et al. (2008). The maturing architecture of the brain's default network. *Proc. Natl. Acad. Sci. U.S.A.* 105, 4028–4032. doi: 10.1073/pnas.0800376105

Garrity, A. G., Pearlson, G. D., Mckiernan, K., Lloyd, D., Kiehl, K. A., and Calhoun, V. D. (2007). Aberrant default mode functional connectivity in schizophrenia. *Am. J. Psychiatry* 164, 450–457. doi: 10.1176/ajp.2007.164.3.450

Greicius, M. D., Srivastava, G., Reiss, A. L., and Menon, V. (2004). Default-mode network activity distinguishes Alzheimer's disease from healthy aging: evidence from functional MRI. *Proc. Natl. Acad. Sci. U.S.A.* 101, 4637–4642. doi: 10.1073/pnas.0308627101

Hampson, M., Driesen, N. R., Skudlarski, P., Gore, J. C., and Constable, R. T. (2006). Brain connectivity related to working memory performance. *J. Neurosci.* 26, 13338–13343. doi: 10.1523/JNEUROSCI.3408-06.2006

Hervais-Adelman, A., Moser-Mercer, B., and Golestani, N. (2015). Brain functional plasticity associated with the emergence of expertise in extreme language control. *Neuroimage* 114, 264–274. doi: 10.1016/j.neuroimage.2015.03.072

Highstein, S. M., Fay, R. R., and Popper, A. N. (2004). *The Vestibular System*, Vol. 24. Berlin: Springer. doi: 10.1007/b97280

Huang, K., and Aviyente, S. (2006). "Sparse representation for signal classification," in *Proceedings of Advances in Neural Information Processing Systems*, (Cambridge, MA: MIT Press), 609–616.

Hutchison, R. M., Womelsdorf, T., Allen, E. A., Bandettini, P. A., Calhoun, V. D., Corbetta, M., et al. (2013). Dynamic functional connectivity: promise, issues, and interpretations. *Neuroimage* 80, 360–378. doi: 10.1016/j.neuroimage.2013.05.079

Hyvärinen, A. (1999). Fast and robust fixed-point algorithms for independent component analysis. *IEEE Trans. Neural Netw.* 10, 626–634. doi: 10.1109/72.761722

Jeong, M., Tashiro, M., Singh, L. N., Yamaguchi, K., Horikawa, E., and Miyake, M. (2006). Functional brain mapping of actual car-driving using [18F] FDG-PET. *Ann. Nucl. Med.* 20, 623–628. doi: 10.1007/BF02984660

Jing, Y., Zeng, W., Wang, N., Ren, T., Shi, Y., Yin, J., et al. (2015). GPU-based parallel group ICA for functional magnetic resonance data. *Comput. Methods Programs Biomed.* 119, 9–16. doi: 10.1016/j.cmpb.2015.02.002

Leonardi, N., Richiardi, J., Gschwind, M., Simioni, S., Annoni, J. M., Schluep, M., et al. (2013). Principal components of functional connectivity: a new approach to study dynamic brain connectivity during rest. *Neuroimage* 83, 937–950. doi: 10.1016/j.neuroimage.2013.07.019

Li, X., Zhu, D., Jiang, X., Jin, C., Zhang, X., Guo, L., et al. (2014). Dynamic functional connectomics signatures for characterization and differentiation of PTSD patients. *Hum. Brain Mapp.* 35, 1761–1778. doi: 10.1002/hbm.22290

Liang, X., Zou, Q., He, Y., and Yang, Y. (2013). Coupling of functional connectivity and regional cerebral blood flow reveals a physiological basis for network hubs of the human brain. *Proc. Natl. Acad. Sci. U.S.A.* 110, 1929–1934. doi: 10.1073/pnas.1214900110

Liu, D., Dong, Z., Zuo, X., Wang, J., and Zang, Y. (2013). Eyes-open/eyes-closed dataset sharing for reproducibility evaluation of resting state fMRI data analysis methods. *Neuroinformatics* 11, 469–476. doi: 10.1007/s12021-013-9187-0

Lynall, M. E., Bassett, D. S., Kerwin, R., McKenna, P. J., Kitzbichler, M., Muller, U., et al. (2010). Functional connectivity and brain networks in schizophrenia. *J. Neurosci.* 30, 9477–9487. doi: 10.1523/JNEUROSCI.0333-10.2010

Mairal, J., Bach, F., Ponce, J., and Sapiro, G. (2010). Online learning for matrix factorization and sparse coding. *J. Mach. Learn. Res.* 11, 19–60. doi: 10.1016/j.neunet.2012.05.003

Majeed, W., Magnuson, M., Hasenkamp, W., Schwarb, H., Schumacher, E. H., Barsalou, L., et al. (2011). Spatiotemporal dynamics of low frequency BOLD fluctuations in rats and humans. *Neuroimage* 54, 1140–1150. doi: 10.1016/j.neuroimage.2010.08.030

Orr, J. M., Turner, J. A., and Mittal, V. A. (2014). Widespread brain dysconnectivity associated with psychotic-like experiences in the general population. *Neuroimage* 4, 343–351. doi: 10.1016/j.nicl.2014.01.006

Petrella, J. R., Sheldon, F. C., Prince, S. E., Calhoun, V. D., and Doraiswamy, P. M. (2011). Default mode network connectivity in stable vs progressive mild cognitive impairment. *Neurology* 76, 511–517. doi: 10.1212/WNL.0b013e31820af94e

Raichle, M. E., and Gusnard, D. A. (2002). Appraising the brain's energy budget. *Proc. Natl. Acad. Sci. U.S.A.* 99, 10237–10239. doi: 10.1073/pnas.172399499

Raichle, M. E., MacLeod, A. M., Snyder, A. Z., Powers, W. J., Gusnard, D. A., and Shulman, G. L. (2001). A default mode of brain function. *Proc. Natl. Acad. Sci. U.S.A.* 98, 676–682. doi: 10.1073/pnas.98.2.676

Ren, H., and Chang, C. I. (2003). Automatic spectral target recognition in hyperspectral imagery. *IEEE Trans. Aerosp. Electron. Syst.* 39, 1232–1249. doi: 10.1109/TAES.2003.1261124

Ren, T., Zeng, W., Wang, N., Chen, L., and Wang, C. (2014). A novel approach for fMRI data analysis based on the combination of sparse approximation and affinity propagation clustering. *Magn. Reson. Imaging* 32, 736–746. doi: 10.1016/j.mri.2014.02.023

Rubinov, M., and Sporns, O. (2010). Complex network measures of brain connectivity: uses and interpretations. *Neuroimage* 52, 1059–1069. doi: 10.1016/j.neuroimage.2009.10.003

Rytty, R., Nikkinen, J., Paavola, L., Abou, E. A., Moilanen, V., Visuri, A., et al. (2013). GroupICA dual regression analysis of resting state networks in a behavioral variant of frontotemporal dementia. *Front. Hum. Neurosci.* 7:461. doi: 10.3389/fnhum.2013.00461

Schwarz, G. (1978). Estimating the dimension of a model. *Ann. Stat.* 6, 461–464. doi: 10.1214/aos/1176344136

Sheline, Y. I., Barch, D. M., Price, J. L., Rundle, M. M., Vaishnavi, S. N., Snyder, A. Z., et al. (2009). The default mode network and self-referential processes in depression. *Proc. Natl. Acad. Sci. U.S.A.* 106, 1942–1947. doi: 10.1073/pnas.0812686106

Shen, H., Li, Z., Qin, J., Liu, Q., Wang, L., Zeng, L. L., et al. (2016). Changes in functional connectivity dynamics associated with vigilance network in taxi drivers. *Neuroimage* 124, 367–378. doi: 10.1016/j.neuroimage.2015.09.010

Shi, Y., Zeng, W., Wang, N., and Chen, D. (2015a). A novel fMRI group data analysis method based on data-driven reference extracting from group subjects. *Comput. Methods Programs Biomed.* 122, 362–371. doi: 10.1016/j.cmpb.2015.09.002

Shi, Y., Zeng, W., Wang, N., Wang, S., and Huang, Z. (2015b). Early warning for human mental sub-health based on fMRI data analysis: an example from a seafarers' resting-data study. *Front. Psychol.* 6:1030. doi: 10.3389/fpsyg.2015.01030

Smith, S. M., Miller, K. L., Moeller, S., Xu, J., Auerbach, E. J., Woolrich, M. W., et al. (2012). Temporally-independent functional modes of spontaneous brain activity. *Proc. Natl. Acad. Sci. U.S.A.* 109, 3131–3136. doi: 10.1073/pnas.1121329109

Sporns, O. (2011). The human connectome: a complex network. *Ann. N. Y. Acad. Sci.* 1224, 109–125. doi: 10.1111/j.1749-6632.2010.05888.x

Tang, X., Zeng, W., Wang, N., and Yang, J. (2015). An adaptive RV measure based fuzzy weighting subspace clustering (ARV-FWSC) for fMRI data analysis. *Biomed. Signal Process. Control* 22, 146–154. doi: 10.1016/j.bspc.2015.07.006

Tung, K. C., Uh, J., Mao, D., Xu, F., Xiao, G., and Lu, H. (2013). Alterations in resting functional connectivity due to recent motor task. *Neuroimage* 78, 316–324. doi: 10.1016/j.neuroimage.2013.04.006

Tzourio-Mazoyer, N., Landeau, B., Papathanassiou, D., Crivello, F., Etard, O., Delcroix, N., et al. (2002). Automated anatomical labeling of activations in SPM using a macroscopic anatomical parcellation of the MNI MRI single-subject brain. *Neuroimage* 15, 273–289. doi: 10.1006/nimg.2001.0978

Van Dijk, K. R., Hedden, T., Venkataraman, A., Evans, K. C., Lazar, S. W., and Buckner, R. L. (2010). Intrinsic functional connectivity as a tool for human connectomics: theory, properties, and optimization. *J. Neurophysiol.* 103, 297–321. doi: 10.1152/jn.00783.2009

Wang, L., Liu, Q., Shen, H., Li, H., and Hu, D. (2015). Large-scale functional brain network changes in taxi drivers: evidence from resting-state fMRI. *Hum. Brain Mapp.* 36, 862–871. doi: 10.1002/hbm.22670

Wang, N., Zeng, W., and Chen, D. (2016a). A novel sparse dictionary learning separation (SDLS) model with adaptive dictionary mutual incoherence constraint for fMRI data analysis. *IEEE Trans. Biomed. Eng.* 63, 2376–2389.

Wang, N., Zeng, W., Chen, D., Yin, J., and Chen, L. (2016b). A novel brain networks enhancement model (BNEM) for BOLD fMRI data analysis with highly spatial reproducibility. *IEEE J. Biomed. Health Inform.* 20, 1107–1119. doi: 10.1109/JBHI.2015.2439685

Wang, N., Zeng, W., and Chen, L. (2012). A Fast-FENICA method on resting state fMRI data. *J. Neurosci. Methods* 209, 1–12. doi: 10.1016/j.jneumeth.2012.05.007

Wang, N., Zeng, W., and Chen, L. (2013). SACICA: a sparse approximation coefficient-based ICA model for functional magnetic resonance imaging data analysis. *J. Neurosci. Methods* 216, 49–61. doi: 10.1016/j.jneumeth.2013.03.014

Wang, N., Zeng, W., Shi, Y., Ren, T., Jing, Y., Yin, J., et al. (2015). WASICA: an effective wavelet-shrinkage based ICA model for brain fMRI data analysis. *J. Neurosci. Methods* 246, 75–96. doi: 10.1016/j.jneumeth.2015.03.011

Wright, J., Yang, A. Y., Ganesh, A., Sastry, S. S., and Ma, Y. (2009). Robust face recognition via sparse representation. *IEEE Trans. Pattern Anal. Mach. Intell.* 31, 210–227. doi: 10.1109/TPAMI.2008.79

Yang, H., Hou, C., Lu, J., Luo, C., and Yao, D. (2016). Functional brain network study on resting state of composers. *Chin. J. Biomed. Eng.* 35, 612–615. doi: 10.1038/srep12277

Yang, M., Zhang, L., Feng, X., and Zhang, D. (2014). Sparse representation based fisher discrimination dictionary learning for image classification. *Int. J. Comput. Vision* 109, 209–232. doi: 10.1007/s11263-014-0722-8

Yao, S., Zeng, W., Wang, N., and Chen, L. (2013). Validating the performance of one-time decomposition for fMRI analysis using ICA with automatic target generation process. *Magn. Reson. Imaging* 31, 970–975. doi: 10.1016/j.mri.2013.03.014

Yu, Q., Erhardt, E. B., Sui, J., Du, Y., He, H., Hjelm, D., et al. (2015). Assessing dynamic brain graphs of time-varying connectivity in fMRI data: application to healthy controls and patients with schizophrenia. *Neuroimage* 107, 345–355. doi: 10.1016/j.neuroimage.2014.12.020

Zhang, D., and Raichle, M. E. (2010). Disease and the brain's dark energy. *Nat. Rev. Neurol.* 6, 15–28. doi: 10.1038/nrneurol.2009.198

Zhang, X., Guo, L., Li, X., Zhang, T., Zhu, D., Li, K., et al. (2013). Characterization of task-free and task-performance brain states via functional connectome patterns. *Med. Image Anal.* 17, 1106–1122. doi: 10.1016/j.media.2013.07.003

Conflict of Interest Statement: The authors declare that the research was conducted in the absence of any commercial or financial relationships that could be construed as a potential conflict of interest.